Low-pressure clino- to high-pressure clino-enstatite phase transition: a phonon related mechanism

YONGGANG G. YU[1*] AND RENATA M. WENTZCOVITCH[2†]

[1] Department of Chemistry, Minnesota Supercomputing Institute,
University of Minnesota, Minneapolis, MN 55455, USA

[2]Department of Chemical Engineering and Materials Sciences,
Minnesota Supercomputing Institute, University of Minnesota, Minneapolis, MN 55455, USA

November 7, 2008

Abstract

We have investigated by first principles the compressional behavior of low-pressure (LP) and high-pressure (HP) $MgSiO_3$ clinoenstatite. We have carefully examined cell shapes, chain angles, and polyhedral volume responses, such as angle variances and quasi-elongations, under pressure at room temperature. We have observed opposite behavior of the tetrahedra in the S-rotated and O-rotated chains with pressure in the LP phase, with a slight increase (decrease) in angle variance and quasi-elongation in the former (latter). Inspection of zone center modes of both phases under pressure reveals a transition path that converts the S-rotated chain in the LP phase into the O-rotated chain in the HP phase. This conversion is related to a slight softening of an A_g "metastable" Raman mode under pressure.

Keywords: phase transition mechanism, low pressure clinoenstatite, high pressure clinoenstatite, Raman, IR, phonon frequency

INTRODUCTION

Next to olivine, pyroxenes including clinopyroxene and orthopyroxene are the most abundant constituents of Earth upper mantle (Ringwood, 1975). It has been suggested (Woodland and Angel, 1997; Woodland, 1998) that the phase

*Corresponding author (email: yonggang@cems.umn.edu). Tel.: +1-612-624-2872; fax: +1-612-626-7246.
†email: wentzcov@cems.umn.edu

transformation of orthopyroxene to high-pressure clinopyroxene may account for the X-discontinuity at 312 ± 21-km depth observed by Revenaugh and Jordan (1991). The progressive dissolution of pyroxene into garnet increases velocity gradients between depths of 300–460-km in Earth as pointed out by Ringwood (1967). Natural pyroxenes under pressure are often used as starting materials to produce perovskite at lower mantle conditions in experimental mineral physics.

Because of their abundance in the upper mantle, the magnesium end member clinopyroxene, $MgSiO_3$ enstatite are among the most investigated minerals under pressure. They exist in the low pressure $P2_1/c$ structure (LP-En hereafter) and high pressure C2/c structure (HP-En hereafter). LP-En exists at ambient conditions while HP-En had eluded unambiguous experimental detection until the 1990s because of its conversion into LP-En structure upon quenching (Angel et al., 1992). In the past few decades, crystal chemistry, equation of state, and thermodynamic properties of LP- and HP-En have been experimentally investigated by single crystal or powder X-ray measurements (Thompson, 1970; Krupka et al., 1985; Angel et al., 1992; Angel and Hugh-Jones, 1994; Kung et al., 2004; Chopelas, 1999; Huang et al., 2000; Lin, 2004), or by molecular dynamics simulations using empirical potentials (Matsui and Price, 1992) and by first principles (Wentzcovitch et al., 1995; Duan et al., 2001). However, the transition mechanism for the conversion of LP-En to HP- En has not been addressed so far. Here we present a comparative study of the compressional behavior of the LP- and HP-En that i) substantially improves previous density functional based zero Kelvin calculations (Wentzcovitch et al., 1995; Duan et al., 2001) and ii) identifies a phonon related mechanism for the LP- to HP-En transition.

Both LP-En ($P2_1/c$) and HP-En (C2/c) exist in monoclinic structures with the unique axis b perpendicular to the other two axes, a and c (Fig. 1). The obtuse monoclinic angle between a and c, β, is about 107° for LP-En and 103° for HP-En at ambient conditions. What makes pyroxene of special interest is the corner sharing SiO_4 tetrahedral chains running through the crystal along the c axis, forming a silicate layer parallel to the a-c plane. By convention these SiO_4 tetrahedral chains in LP-En were divided into two types: the "O-rotated" chain (O-chain) and the "S-rotated" chain (S-chain) based on the O_3-O_3-O_3 chain extension angle. This classification characterizes the way these chains promenade along the c direction. LP-En contains both S-chain and O-chain with O_3-O_3-O_3 angles of $\sim 205^\circ$ in the former and $\sim 132^\circ$ in the latter. To illustrate the transition path mentioned above we choose a counter-clockwise chain extension angle as shown in Fig. 1. In HP-En only the O-chain exists and the O_3-O_3-O_3 angle is $\sim 134^\circ$ at ambient conditions. Upon a phase transition from LP-En to HP-En at $\sim$5–8 GPa, the S-chain in LP-En transforms to the O-chain in HP-En. In the next section we introduce the computational method used in this work. Section 3 reports a detailed comparison of the compression behavior of LP-En and HP-En. In section 4 we propose the LP-En to HP-En transition mechanism related to a slight softening of the lowest Raman mode in LP-En. Concluding remarks

are presented in section 5.

COMPUTATIONAL METHOD

We have used density functional theory (DFT) (Hohenberg and Kohn, 1964; Kohn and Sham, 1965) within the local density approximation (LDA) (Ceperley and Alder, 1980) as parametrized by Perdew and Zunger (1981). The pseudopotentials used here have been successfully applied to phase transitions such as perovskite to postperovskite (Tsuchiya et al., 2004) and the postspinel dissociation (Yu et al., 2007) in magnesium silicates. The magnesium pseudopotential was generated by the method of von Barth and Car, which replaces a norm-conversing Mg pseudopential used by (Wentzcovitch et al., 1995; Duan et al., 2001) to study HP-En and LP-En in $MgSiO_3$. The oxygen and silicon pseudopotentials were generated by the method of Troullier and Martins (1991). The plane-wave kinetic energy cutoff ($E_{\rm cut}$) was chosen to be 80 Ry, and a $4 \times 4 \times 4$ Monkhorst and Pack (1976) k-point mesh with $(\frac{1}{2}\frac{1}{2}\frac{1}{2})$ shift from origin was used for Brillouin zone (BZ) samplings of both phases. This ensures the energy convergence with respect to $E_{\rm cut}$ and k-mesh to be within 2.0×10^{-4} Ry/atom. For high pressure structural relaxations, we have adopted the same variable-cell shape molecular dynamics (VCSMD) method (Wentzcovitch, 1991) used in previous DFT studies (Wentzcovitch et al., 1995; Duan et al., 2001). We have calculated Γ-point phonon frequencies using density functional perturbation theory (Baroni et al., 2001). The room temperature structural parameters reported here were obtained by high temperature statically constrained quasiharmonic approximation (QHA) (Carrier et al., 2007). Whole phonon dispersions and complete thermodynamics results will be reported somewhere else.

COMPRESSIONAL BEHAVIOR

Fig. 2 shows the pressure dependence of cell parameters of LP- and HP-En from this study at 300 K using statically constrained QHA, from previous static DFT calculations by Duan et al. (2001), and from room temperature experimental measurements by Angel et al. (1992); Angel and Hugh-Jones (1994). In fact the ability of the QHA to produce structural parameters has only recently been recognized (Carrier et al., 2007). Compared to the previous LDA results by Duan et al. (2001), the current ones agree considerably better with experimental data. To a great extent this owes to the inclusion of lattice vibrational effects that expand the static lattice parameters. But this is not all. The magnesium pseudopotentials used here is more transferable also. As can be seen, the c axis is quite stiffer than the a and b axes for both LP- and HP-En. Only a small reduction in the monoclinic angle β with pressure is observed in both phases. Across the LP-En to HP-En transformation at $\sim$ 7 GPa (Angel et al. (1992)), abrupt reductions of the a and c axes

and of the monoclinic angle, β, are observed. This results in a primitive cell volume reduction from 393.2 Å^3 to 383.3 Å^3 and in a density increase of $\sim 2.8\%$. **A detailed comparison of LDA calculated 300 K unit cell parameters for LP-En (ambient pressure) and HP-En (7.9 GPa) with previous experimental and theoretical studies is shown in Table 1.**

The chain angles in LP- and HP-En (defined in Fig. 1) at 300 K and up to 30 GPa are shown in Fig. 3. In both phases we observe a monotonic decrease of the angles in the O-chains (O_3-O_3-O_3 and Si-O_3-Si angles). In LP-En (Fig. 3(a)) the O_3-O_3-O_3 angle in the S-chain is $\sim 20^\circ$ larger than that angle in the O-chain at all pressures investigated. For HP-En, we plot the three different bond angles in the O-chain in Fig. 3(b) together with experimental data (Angel et al., 1992) and angles reported by a previous static LDA calculation (Wentzcovitch et al., 1995). Our bond angles at 300 K agree better with experiments than the previous static one by Wentzcovitch et al. (1995) owing to vibrational effects and to the more accurate magnesium pseudopotential (von Barth and Car) used here.

The 300 K polyhedral volumes under pressure are shown in Fig. 4. In average, the compressibility, $\kappa = -\frac{1}{V}\frac{\partial V}{\partial P}$, of MgO_6 octahedra is ~ 3 times larger than that of SiO_4 tetrahedra. To quantify the degree of polyhedral distortion under compression, we have computed angle variances (AV) and quadratic elongations (QE) (Robinson et al., 1971). AV is defined as the variance of bond angles from their ideal values, i.e., $\sigma^2_{\rm oct} = \sum_{i=1,12}(\theta_i - 90^\circ)^2/11$ for an octahedron and $\sigma^2_{\rm tet} = \sum_{i=1,6}(\theta_i - 109.47^\circ)^2/5$ for a tetrahedron. θ is the angle between bonds defined by atoms located at the corner and at the center of these polyhedra. QE is the mean quadratic elongation of a polyderon's bond lengths (l_i) from those of an ideal polyhedron with the same volume and a single bond length (l_0), i.e. $\lambda_{\rm oct} = \sum_{i=1,6}(l_i/l_0)^2/N$, with $N = 6$ ($N = 4$) for an octahedron (tetrahedron).

Fig. 5 displays the calculated AV and QE for polyhedra in LP- and HP-En. Two prominent features appear in LP-En (Fig. 5 (a)). First, among the four types of polyhedra, i.e., M1 and M2 octahedra and S- and O-type tetrahedra, the M2 octahedron is the most distorted. This is indicated by very large AV and QE values of this polyhedron. Second, with increasing pressure, the S-type tetrahedron becomes more distorted, while all other polyhedra become more regular under pressure. This suggested a potential instability of the S-type chain in LP-En. The M2 octahedra in HP-En are much more regular (smaller AV and QE) than the M1 and M2 octahedra in LP-En. Next we discuss long wavelength lattice vibrations, that tell, in this case, more than macroscopic compression mechanisms about structural instabilities.

ZONE CENTER MODES AND THE TRANSITION MECHANISM

The calculated zone center phonon frequencies of LP- and HP-En are displayed at several (static) pressures and compared with available room temperature high pressure experimental Raman and IR data (Chopelas, 1999; Huang et al., 2000; Lin, 2004) in Fig. 6. The colored lines are from this calculation and the black solid lines are Raman frequency vs. pressure fittings at room temperature by Lin (2004). Symbols in Fig. 6(a) are from Raman data at 0 GPa by Lin (2004), while those in Fig. 6(b) are from Raman data at 12.5 GPa by Chopelas and Boehler (1992). They are in very good agreement with our predictions.

An interesting point shown in Fig. 6 is that, except for the lowest Raman mode with A_g symmetry, the frequencies of all other modes in LP-En increase with pressure. The softening of the lowest A_g mode with pressure suggests a structural instability related to this mode. **In specific, the phonon frequency of the lowest A_g Raman mode decreases from 125.8 to 124.1 to 119.7 cm^{-1} when pressure is increased from 0 to 5 to 10 GPa, respectively. Notice that according to Angel et al. (1992), LP-En is metastable with respect to HP-En above 5.34–7.93 GPa. 5.34 and 7.93 refer to decompression and compression transition pressures respectively.** Closer inspection of the atomic displacements (eigenvector) associated with this mode reveals that it folds the S-chain away from the O-chain and reduces the O_3-O_3-O_3 S-chain angle. We investigate the effect of this mode on the structure of LP-En by adding the atomic displacements corresponding to the A_g mode to each atom in fully relaxed LP-En structure with $P2_1/c$ symmetry at (static) 5 GPa, where cell parameters are 9.287 Å(a), 8.438 Å(b), 4.992 Å(c), and 107.3° (β) (Fig. 7(a)). We produce an intermediate structure (Fig. 7(b)) with the same $P2_1/c$ symmetry in which the O3-O3-O3 S-chain angle ($\theta_{\text{s-chain}}$ hereafter) is smaller than in the starting configuration ($\sim 207°$). A subsequent relaxation of the entire crystal structure at 5 GPa using VCSMD leads to the C2/c HP-En structure (Fig. 7(c)), a structure whose space group is a super group of $P2_1/c$. We conclude that the transition path should be along this A_g normal mode displacement, because, as we will demonstrate, the effect of this mode is to release the internal pressure (stress) at fixed volume and reduce the enthalpy of the crystal. Here it should be noted that our starting LP-En configuration at 5 GPa is actually unstable relative to the HP-En configuration, because the LDA static transition pressure for the LP- to HP-En transition is found to be 1.8 GPa.

Plotted in Fig. 8 are the dependences of $\theta_{\text{s-chain}}$ on A_g mode amplitude and of the enthalpy on $\theta_{\text{s-chain}}$ at various monoclinic cell angles β (see caption in Fig. 8). The $P2_1/c$ symmetry comprising 4 point group operations is found for all displaced configurations when the A_g mode is applied to LP-En. Meanwhile $\theta_{\text{s-chain}}$ decreases monotonically with increasing mode amplitude (at 5 GPa with fixed cell shape) and the static enthalpy of the crystal decreases to a local minimum at about $\theta_{\text{s-chain}}$=145° before it increases again rapidly, irrespective of β. The enthalpy vs. $\theta_{\text{s-chain}}$ curves

were generated by varying only two degrees of freedom in the structure equilibrated at 5 GPa: $\theta_{\text{s-chain}}$, through the application of the A_g mode displacement, and β, the monoclinic cell angle. No structural relaxation was performed at this point. This plot indicates that, indeed, the displacement of atoms according to the A_g mode decreases the enthalpy at 5 GPa. This is because along this path where the $\theta_{\text{s-chain}}$ varies from $\sim 205^\circ$ to $\sim 145^\circ$ to $\sim 125^\circ$ with increasing mode amplitude at $\beta = 107^\circ$, the internal pressure decreases from the initial pressure, 5 GPa, to -4 GPa, where enthalpy is lowest, and then increase again. Similar trend was observed at other fixed angles β. The consequence is a dramatic decrease then a rapid increase in static enthalpy with increasing A_g mode amplitude (or with decreasing $\theta_{\text{s-chain}}$). Therefore this appears to be a viable path for the LP- to HP-En transition. As mentioned above, structural relaxation after application of this mode to LP-En at 5 GPa leads to the HP-En. This is not a soft mode transition and the A_g mode frequency decreases only slightly before the transition takes place. Instead, the chain rotation leading from LP- to HP-En is a discontinuous, first order, enthalpically driven event that could take place along the path provided by the A_g displacement mode. Other paths are not ruled out at this point, but current result strongly suggests that the transformation mechanism is related with this phonon mode.

CONCLUDING REMARKS

We predict by first principles the high pressure behavior of low pressure (LP-) and high pressure (HP-) enstatites (EN). Using an improved pseudopotential for magnesium and including vibrational effects we find excellent agreement between our predicted LDA structural parameters at 300 K and the experimentally determined ones. By investigating angle variances (AV) and quadratic elongations (QE) of all polyhedra in these structures, we notice that the SiO_4 tetrahedra in the S-type chain in LP-En become increasingly distorted under pressure, in direct contrast with the other polyhedra that become more regular under compression. This suggests a structural instability associated with this chain. Investigation of the zone center phonon frequencies reveals that the frequency of the lowest Raman mode with A_g symmetry decreases slightly with pressure, in contrast to the behavior of all other zone center modes whose frequencies increase with pressure. Inspection of the atomic displacements associated with the metastable A_g mode reveals a direct path between the LP- and HP- En structures. Other paths are not ruled out at this point, but the current result strongly suggests that the transformation mechanism is related with this zone center phonon mode.

ACKNOWLEDGMENTS

This research was supported by NSF grants: Earth-0230319, Earth-0635990, and ATM-0428774. Computations were performed at the Minnesota Supercomputing Institute.

Table 1: LDA calculated 300 K unit cell parameters of $MgSiO_3$ LP-En (ambient pressure) and HP-En (7.9 GPa) compared with previous experiments and theoretical calculations.

		a (Å)	b (Å)	c (Å)	$\beta(^\circ)$	V(Å^3/uc)
LP-En	this work	9.591	8.809	5.165	107.95	415.2
	Ohashi (1984)	9.606	8.8131	5.170	108.35	415.5
	Angel and Hugh-Jones (1994)	9.605	8.814	5.169	108.34	415.5
	Matsui and Price (1992)	9.600	8.672	5.244	108.60	413.8
	Duan et al. (2001)	9.4876	8.6682	5.1050	107.90	399.5
HP-En	this work	9.186	8.620	4.907	101.0	381.4
	Wentzcovitch et al. (1995)	9.12	8.19	4.904	101.3	359.2
	Angel et al. (1992)	9.201	8.621	4.908	101.50	381.5

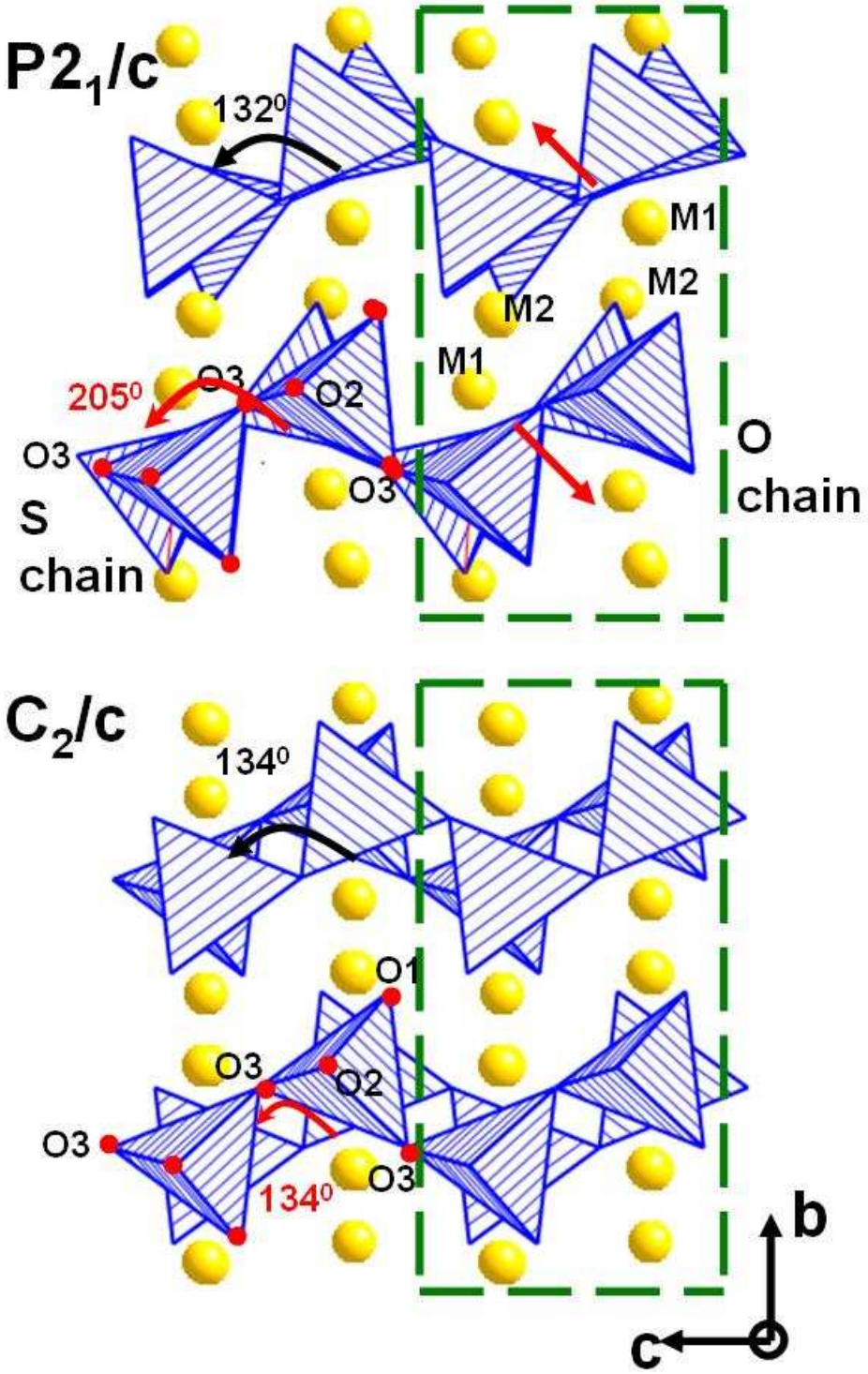

Figure 1: Crystal structures of $MgSiO_3$ in the LP-En ($P2_1/c$) and HP-En (C2/c) phases at 0 GPa.

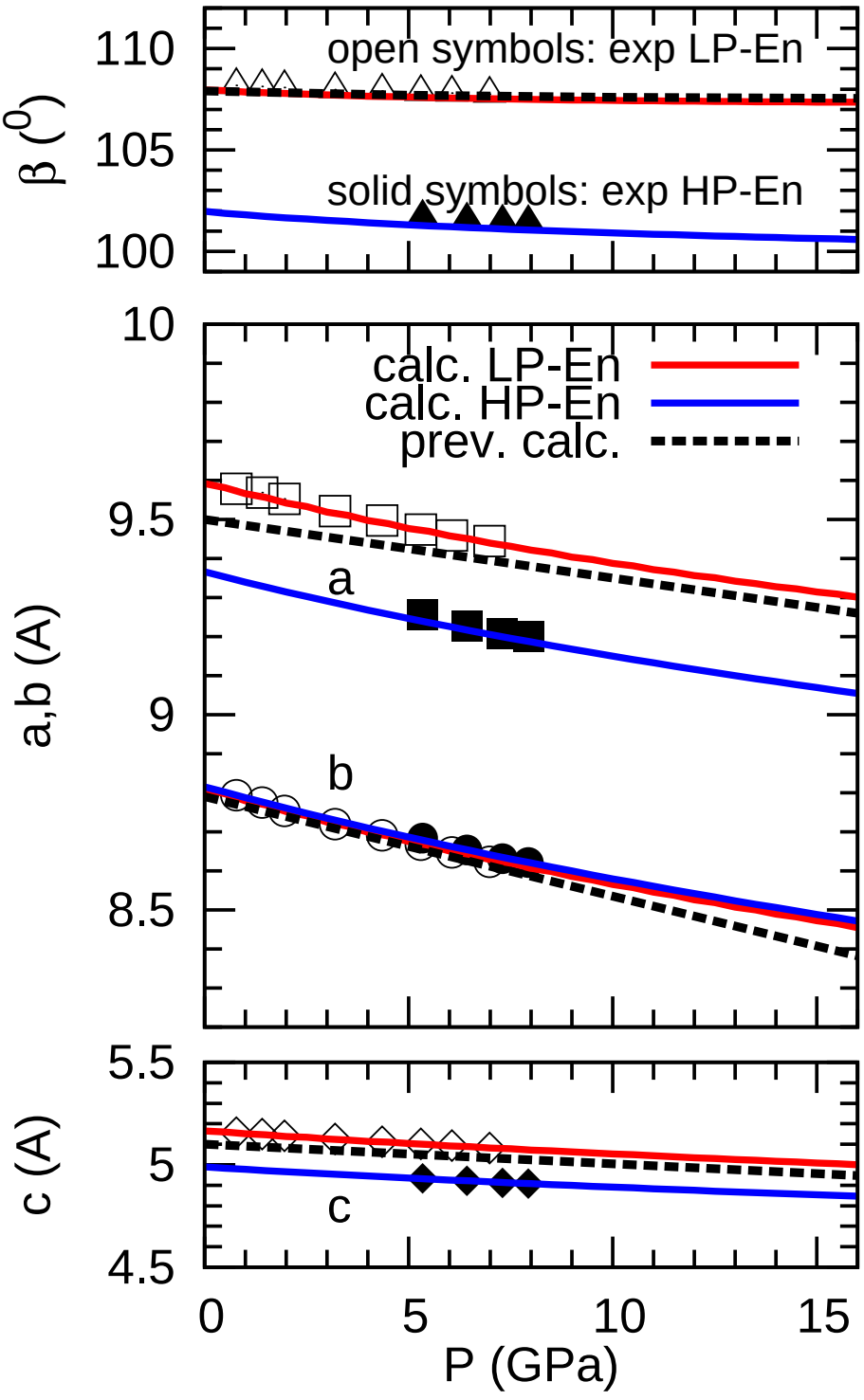

Figure 2: Predicted pressure dependence of the lattice parameters of LP- and HP-En at 300 K, compared with experimental measurements (Angel and Hugh-Jones (1994) in symbols) and previous static LDA calculation of LP-En (Duan et al. (2001) in dashed lines).

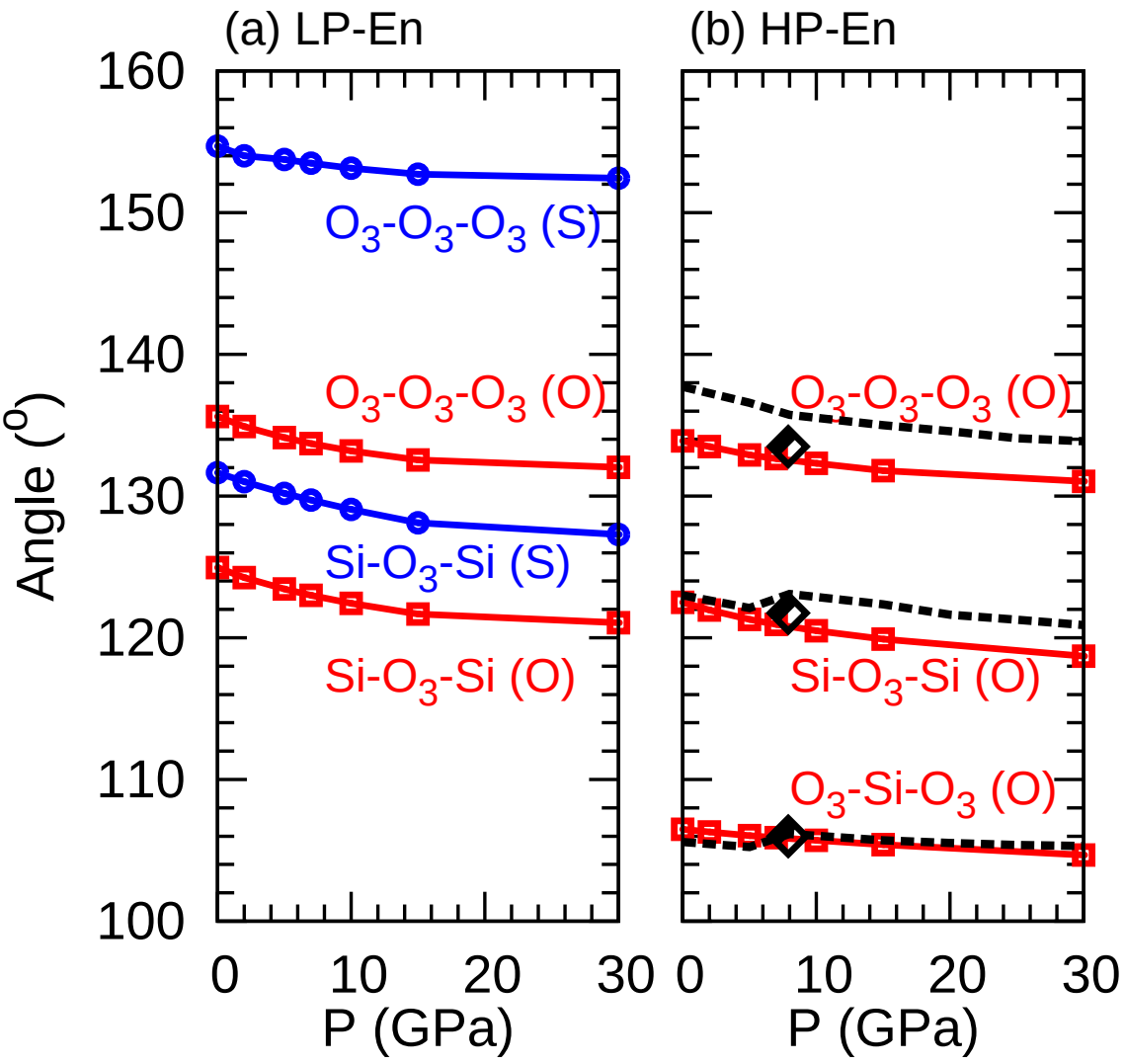

Figure 3: Variation of tetrahedral chain angles (see Fig. 1) with pressure. Diamond symbols denote experimental data (Angel et al., 1992) and dashed lines represent previous static calculations (Wentzcovitch et al., 1995).

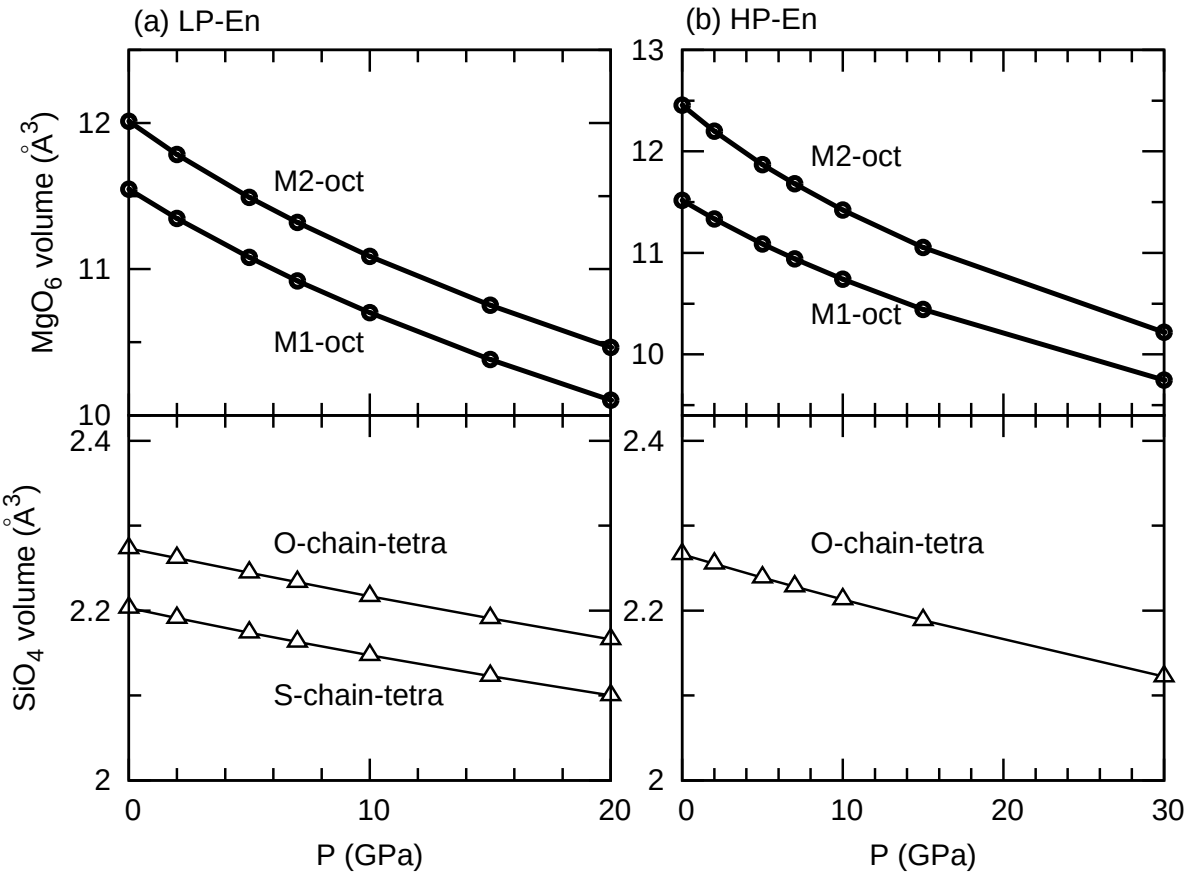

Figure 4: Predicted variation of polyhedral volume with pressure at 300 K in LP- and HP-En.

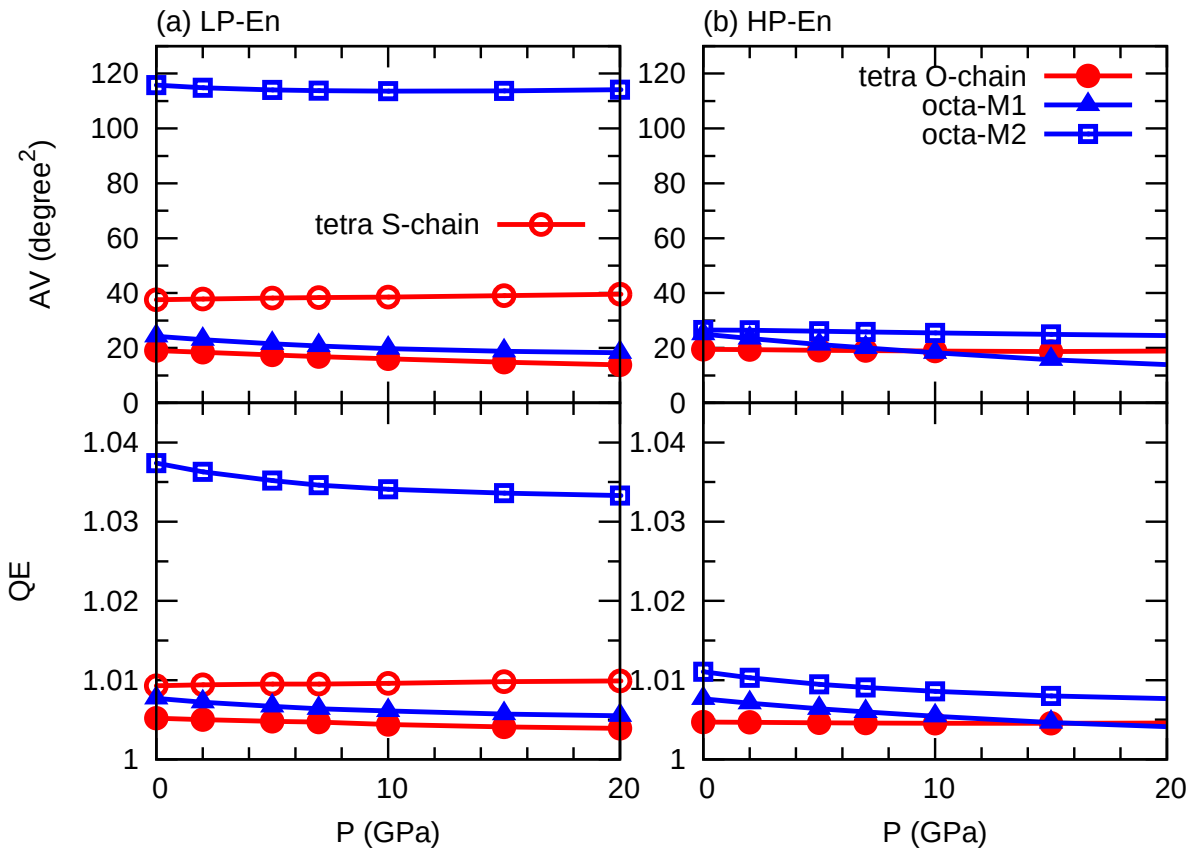

Figure 5: Prediction of polyhedral angle variance (AV) and quasi-elongation (QE), defined in Sec. in LP- and HP-En under pressure at 300 K.

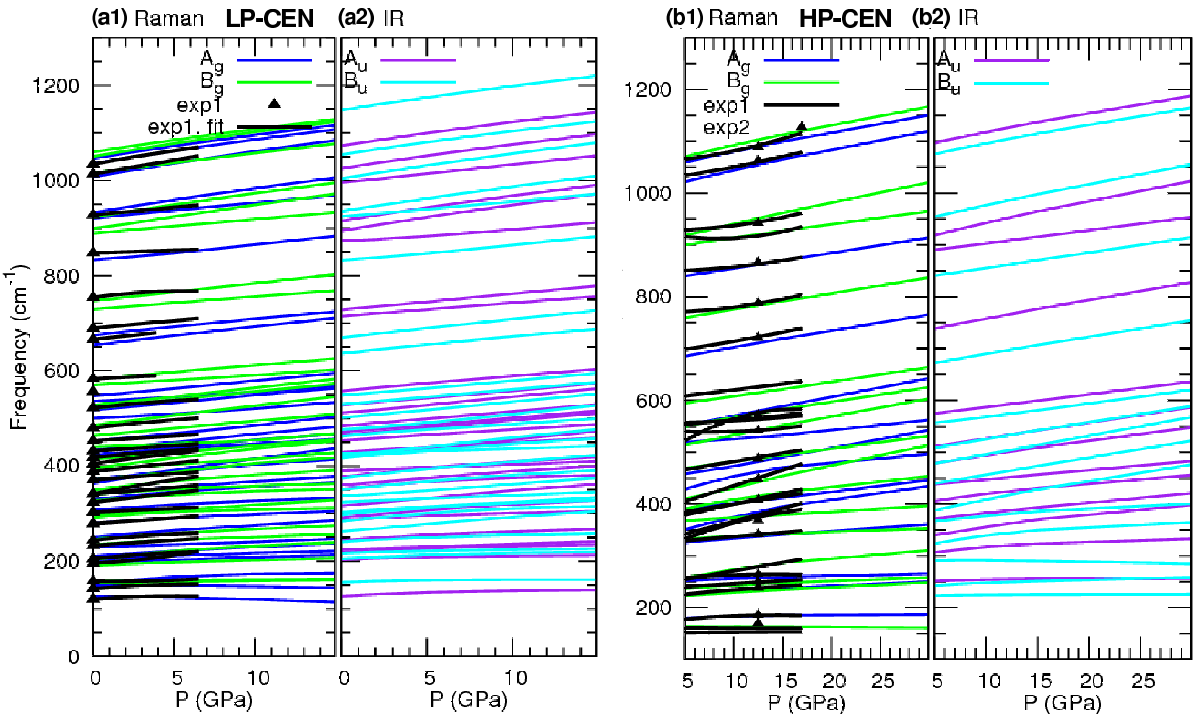

Figure 6: Predicted pressure dependence of Raman and IR frequency of LP- and HP-En at 0 K compared to experimental data (exp1=Lin (2004) and exp2=Chopelas (1999)).

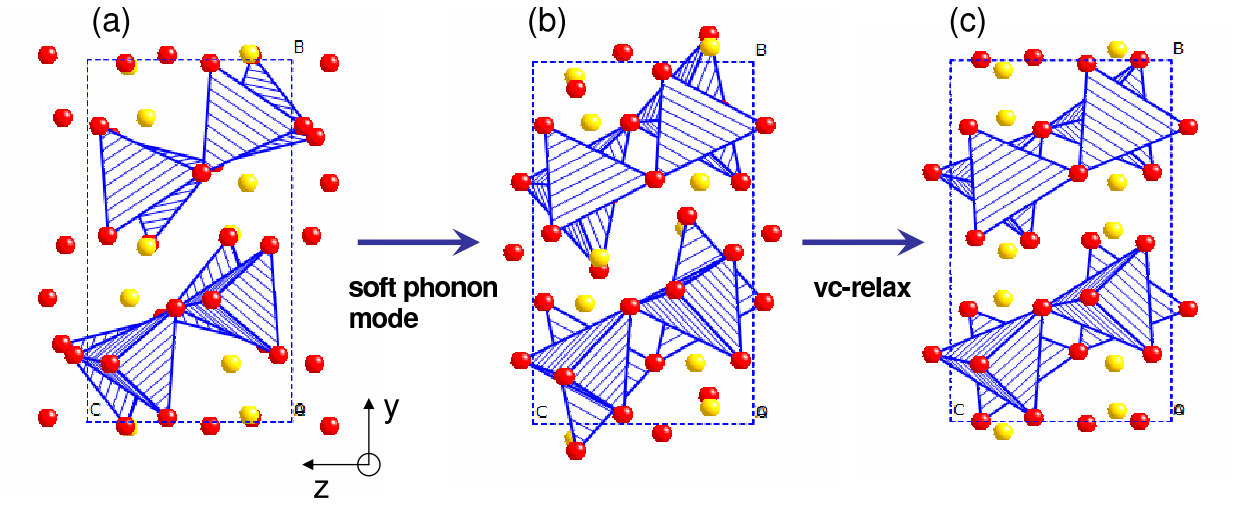

Figure 7: (a) $P2_1/c$ LP-En structure at 5 GPa whose cell parameters a, b, c, and β are 9.47 Å, 8.67 Å, 5.1 Å, and 107.6°, respectively; (b) intermediate structure resulting from the superposition of the A_g mode displacement (see text) to the $P2_1/c$ structure shown in (a); (c) C2/c HP-En structure with new cell-parameters a, b, c, and β equal respectively to 9.24 Å, 8.68 Å, 4.93 Å, and 101.3° that results from the complete structural relaxation at 5 GPa using VCSMD (Wentzcovitch, 1991).

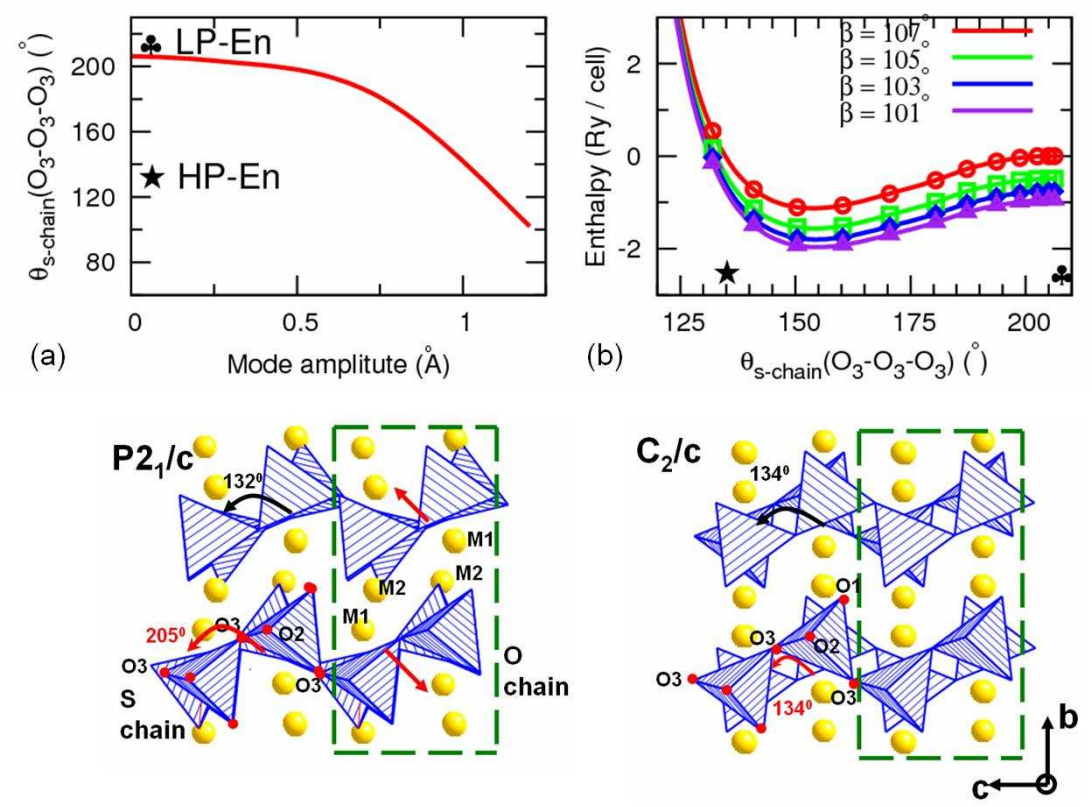

Figure 8: (a) Effect of A_g mode displacement amplitude on S-chain rotation angle ($\theta_{\text{s-chain}}(O_3 - O_3 - O_3)$) of LP-En and (b) how this S-chain rotation angle affects the static enthalpy of this structure at various monoclinic cell angles β. Enthalpy is plotted relative to the static enthalpy of fully relaxed LP-En at 5 GPa (static). (40 atoms exist in one unit cell in LP-En).

References

Angel, R. J., Chopelas, A., Ross, N. L. (1992) Stability of high-density clinoenstatite at upper-mantle pressures. Nature, 358, 322–324.

Angel, R. J., Hugh-Jones, D. A. (1994) Equations of state and thermodynamic properties of enstatite pyroxenes. Journal of Geophysical Research, 99, 19777–19783.

Baroni, S., de Gironcoli, S., Corso, A. D., Giannozzi, P. (2001) Phonons and related crystal properties from density-functional perturbation theory. Reviews of Modern Physics, 73, 515–562.

Carrier, P., Wentzcovitch, R., Tsuchiya, J. (2007) First-principles prediction of crystal structures at high temperatures using the quasiharmonic approximation. Physical Review B, 76 (6), 064116.

Ceperley, D. M., Alder, B. J. (1980) Ground state of the electron gas by a stochastic method. Physical Review Letters, 45, 566–569.

Chopelas, A. (1999) Estimates of mantle relevant Clapeyron slopes in the $MgSiO_3$ system from high-pressure spectroscopic data. American Mineralogist, 84, 233–244.

Chopelas, A., Boehler, R. (1992) Raman spectroscopy of high pressure $MgSiO_3$ phases synthesized in a CO_2 laser heated diamond anvil cell: Perovskite and clinopyroxene. In: Syono, Y., Manghnani, M. (Eds.), High Pressure Research: Application to Earth and Planetary Sciences. Terra Scientific Publ. Co., pp. 101–108.

Duan, W. H., Karki, B. B., Wentzcovitch, R. M., Gu, B. L. (2001) Ab initio study of $mgsio_3$ low-clinoenstatite at high pressure. American Mineralogist, 86, 762–766.

Hohenberg, P., Kohn, W. (1964) Inhomogeneous Electron Gas. Physical Review, 136, 864–871.

Huang, E., Chen, C. H., Huang, T., Lin, E. H., Xu, J. (2000) Raman spectroscopic characteristics of Mg-Fe-Ca pyroxenes. American Mineralogist, 85 (3-4), 473–479.

Kohn, W., Sham, L. J. (1965) Self-Consistent Equations Including Exchange and Correlation Effects. Physical Review, 140, 1133–1138.

Krupka, K. M., Hemingway, B. S., Robie, R. A., Kerrick, D. M. (1985) High-temperature heat capacities and derived thermodynamic properties of anthophyllite, diopside, enstatite, dolomite, bronzite, talc, tremolite, and wollastonite. American Mineralogist, 70, 261–271.

Kung, J., Li, B., Uchida, T., Wang, Y., Neuville, D., Liebermann, R. C. (2004) In situ measurements of sound velocities and densities across the orthopyroxene – high-pressure clinopyroxene transition in $MgSiO_3$ at high pressure. Physics of the Earth and Planetary Interiors, 147, 27–44.

Lin, C.-C. (2004) Pressure-induced polymorphism in enstatite ($MgSiO_3$) at room temperature: clinoenstatite and orthoenstatite. Journal of Physics and Chemistry of Solids, 65, 913–921.

Matsui, M., Price, G. D. (1992) Computer simulation of the $mgsio_3$ polymorphs. Physics and Chemistry of Minerals, 18, 365–372.

Monkhorst, H. J., Pack, J. D. (1976) Special points for Brillouin-zone integrations. Physical Review B, 13, 5188–5192.

Ohashi, Y. (1984) Polysynthetically-twinned structures of enstatite and wollastonite. Physics and Chemistry of Minerals, 10, 217–229.

Perdew, J., Zunger, A. (1981) Self-interaction correction to density-functional approximations for many-electron systems. Physical Review B, 23 (10), 5048–5079.

Revenaugh, J., Jordan, T. H. (1991) Mantle layering from ScS reverberations. 2. The Transition zone. Journal of Geophysical Research, 96 (B12), 19763–19780.

Ringwood, A. E. (1967) The pyroxene-garnet transformation in the earth's mantle. Earth and Planetary Science Letters, 2, 255–263.

Ringwood, A. E. (1975) Composition and petrology of the earth's mantle. McGraw-Hill, New York, Ch. 14-3.

Robinson, K., Gibbs, G. V., Ribbe, P. H. (1971) Quadratic Elongation: A Quantitative Measure of Distortion in Coordination Polyhedra. Science, 172, 567–570.

Thompson, J. B. (1970) Geometric possibilities of amphibole structures and biopyroboles. American Mineralogist, 55, 292–293.

Troullier, N., Martins, J. L. (1991) Efficient pseudopotentials for plane-wave calculations. Physical Review B, 43, 1993.

Tsuchiya, T., Tsuchiya, J., Umemoto, K., Wentzcovitch, R. M. (2004) Phase transition in $MgSiO_3$ perovskite in the earth's lower mantle. Earth and Planetary Science Letters, 224, 241–248.

von Barth, U., Car, R., . Unpublished, briefly described in A. Dal Corso, S. Baroni, R. Resta, and S. de Gironcoli (1993) Physical Review B, 47, 3588.

Wentzcovitch, R. M. (1991) Invariant molecular-dynamics approach to structural phase transitions. Physical Review B, 44, 2358–2361.

Wentzcovitch, R. M., Hugh-Jones, D. A., Angel, R. J., Price, G. D. (1995) Ab-initio study of mgsio$_3$ c2/c enstatite. Physics and Chemistry of Minerals, 22, 453–460.

Woodland, A., Angel, R. (1997) Reversal of the orthoferrosilite-high-P clinoferrosilite transition; a phase diagram for $FeSiO_3$ and implications for the mineralogy of the Earth's upper mantle. European Journal of Mineralogy, 9 (2), 245–254.

Woodland, A. B. (1998) The orthorhombic to high-P monoclinic phase transition in Mg-Fe pyroxenes: Can it produce a seismic discontinuity? Geophysical Research Letters, 25 (8), 1241–1244.

Yu, Y. G., Wentzcovitch, R. M., Tsuchiya, T., Umemoto, K., Weidner, D. J. (2007) First principles investigation of the postspinel transition in Mg_2SiO_4. Geophysical Research Letters, 34, 10306.